Synthesis of Zeolites from Greek Fly Ash and Assessment of Their Copper Removal Capacity

Aikaterini Vavouraki [1],*, Georgios Bartzas [2] and Konstantinos Komnitsas [1]

[1] School of Mineral Resources Engineering, Technical University of Crete, 73100 Chania, Greece; komni@mred.tuc.gr

[2] School of Mining and Metallurgical Engineering, National Technical University of Athens, 15780 Athens, Greece; gbartzas@metal.ntua.gr

* Correspondence: avavouraki@isc.tuc.gr; Tel.: +30-28210-06167

check for updates

Abstract: The objective of this study was to synthesize zeolites through fusion of lignite fly ash and NaOH or KOH pellets at 600 °C and assess their removal efficiency in terms of decontamination of solutions containing Cu(II) ions. The removal efficiency of the produced zeolites was tested in batch kinetic experiments using different zeolites and Cu(II) ion concentrations. Experimental data revealed that zeolites synthesized with the use of NaOH exhibited higher removal efficiency compared with those synthesized with the use of KOH. Kinetic data showed that the pseudo-second-order equations described well the removal process. Copper removal was mainly accomplished through the concerted action of chemisorption and intraparticle diffusion. Analytical techniques involving XRF, XRD, FTIR, SEM/EDS and XPS were used for the characterization and morphology analysis of the produced zeolites. SEM/EDS confirmed the presence of copper on the zeolite surface. XPS spectra of Cu2p at 934.3 eV proved the presence of Cu(II) oxidation state, confirming the possible formation of CuO and/or Cu-Cl.

Keywords: fly ash; synthetic zeolites; copper removal; kinetics; XPS

1. Introduction

The dependence of the society on coal-based energy is still high in most countries [1]. Today, coal provides almost 30% of the world's non-renewable primary energy, whereas this figure is anticipated to drop by only 3–4% within the next few years. As a result of coal combustion in power plants, huge quantities of coal fly ash (FA) are generated causing immense management and environmental problems [2]. The generation of electricity in Greece mainly depends (~73%) on the combustion of local lignite, while the most important lignite centers in the country are Ptolemais-Amynteon and Megalopolis, which are located in West Macedonia and Peloponnese regions, respectively. Annually, the electricity generation power plants in Greece burn approximately 64 million tons of lignite and produce nearly 13 million tons of FA [3].

Fly ash mainly consists of aluminosilicates (Al_2O_3 and SiO_2), Fe_2O_3, and CaO and may exhibit toxicity and/or cause environmental and health impacts if not properly managed or disposed of in abandoned lignite quarries and other improper sites [4]. Due to its pozzolanic properties, FA can be used in a number of applications including partial replacement of cement during the production of concrete [5], the production of ceramics and glass-ceramics [6], and the production of alkali-activated materials (AAMs; so-called "inorganic polymers" or "geopolymers"). AAMs can be also used as backfill in exhausted underground mines [7,8], as soil amendment [9], as catalysts in various environmental applications [10], in wastewater treatment [11], as well as for the stabilization of sludge(s) and other hazardous wastes [12].

An interesting option to utilize FA includes its conversion to zeolites, which are microporous hydrated aluminosilicate materials and have high added value [13]. Zeolites have an infinitely extended three-dimensional network consisting of $(SiO_4)^{4-}$ and $(AlO_4)^{5-}$ tetrahedra linked by shared oxygen atoms. The voids and internal channels present in the zeolite network allow easy access and fast diffusion rates of molecules, thus rendering the zeolites as efficient adsorbents for various contaminants [14]. Zeolites can be used in several environmental applications, including removal of heavy metal ions and other inorganic and organic contaminants from municipal, agricultural, mining, metallurgical, and various other industrial wastewaters [15–21]. Zeolites may also be used to remove inorganic and organic air pollutants, including nitrogen oxides (NOx) and volatile organic compounds (VOCs) [22–24]. Finally, they can be used for the removal, fixation, and control of contaminants and transport of nutrients in soils and sediments [25–28].

The main aims of this study were the production of zeolites through fusion of a low-calcium Greek lignite FA with the use of NaOH and KOH, and the determination of their high removal capacity in terms of removing high concentrations of Cu(II) ions from solutions and their morphology using several analytical techniques including surface-sensitive X-ray photoelectron spectroscopy (XPS).

2. Materials and Methods

2.1. Raw Materials and Reagents

The FA used for the synthesis of zeolites was obtained from the Greek thermoelectric power plant of Megalopolis (Peloponnese, Greece). Prior to use, FA was pulverized in a Sepor-type rod mill (Sepor, Los Angeles, CA, USA) to a particle size less than 200 μm. For the fusion tests, analytical-grade NaOH or KOH pellets (Fluka) were used. For the kinetic tests, solutions of copper nitrate trihydrate and sodium chloride were prepared from the corresponding crystalline solids $Cu(NO_3)_2 \cdot 3H_2O$ (Alfa Aesar, Haverhill, MA, USA) and NaCl (Panreac, Barcelona, Spain), respectively, with the use of deionized water (Zalion, London, UK).

2.2. Synthesis of Zeolites

Zeolites were synthesized through fusion of FA with NaOH or KOH in an N-8L SELECTA oven (J.P. Selecta, Barcelona, Spain) at 600 °C for 1 h, using a heating rate of ~10 °C·min^{-1}. The mass ratios of FA to NaOH or KOH were 1:1 (for the production of ZFA1Na and ZFA1K zeolites, respectively) and 1:1.5 (for the production of ZFA1.5Na and ZFA1.5K zeolites, respectively). The produced zeolites were first cooled at room temperature and then pulverized and homogenized using an agate mortar and pestle. The pulverized material was mixed with deionized water in a 500 mL conical flask, using a solid-to-liquid ratio of 20% *w/v*, and stirred for 12 h with the use of a magnetic stirrer (Agimatic-ED; J.P. Selecta). After that, the suspension was further incubated under stirring at 30 °C for 4 days. The synthetic zeolites were obtained after centrifugation in a bench top Nüve NF1200 centrifuge (Nüve, Ankara, Turkey) and drying at 80 °C in a laboratory oven (ON-02G; Jeio Tech, Seoul, Korea) for 24 h. Prior to use, synthetic zeolites were washed with 0.1 M HCl.

2.3. Kinetic Studies

First, the removal efficiency of the produced Na (ZFA1Na and ZFA1.5Na) and K zeolites (ZFA1K and ZFA1.5K) was tested, using a zeolite dosage of 0.5 g·L^{-1} and different initial Cu(II) concentrations, varying from 50 to 400 mg·L^{-1}.

Then, kinetic experiments were carried out to assess the effect of initial Cu(II) concentration (45–200 mg·L^{-1}), using both the Na-based zeolites at dosages 0.3, 0.5, 1.0, and 1.5 g·L^{-1}, on the degree of copper removal. The suspensions (3 mL aliquots) were taken at predefined time intervals (5, 10, 15, 20, 30, and 60 min), filtered using syringe filters (0.45 μm pore size, Polytetrafluoroethylene (PTFE), Chromafil) and analyzed with inductively-coupled plasma mass spectrometry (ICP-MS) in order to determine the residual metal ion concentration. All tests were carried out in conical flasks, with an

operating volume of 250 mL, at a constant ionic strength of 0.1 M NaCl and room temperature (25 ± 1 °C) under stirring at 600 rpm using a magnetic stirrer (Agimatic-ED; J.P. Selecta, Barcelona, Spain).

The evolution of suspension pH was also determined using a Hanna 211 pH/Eh meter (Hanna, Bedfordshire, UK); it is mentioned that pH is relatively constant during the implementation of the tests ($pH_{initial}$ 4.2 and pH_{final} 5.5). At such pH values, no precipitation of $Cu(OH)_2$ is anticipated. However, atacamite and CuO formation may occur according to PHREEQC code v.3.4.0 [29] simulations carried out using the minteq.v4 database and shown in the Supplementary Material (Figure S1). In this context, the calculation of saturation indices (SI) at different pH values revealed that the solution was undersaturated with respect to $Cu(OH)_2$ and $Cu_2(OH)_3NO_3$, and supersaturated with respect to atacamite ($Cu_2(OH)_3Cl$) and CuO at pH values above 4.9 and 5.3, respectively. A negative value of the saturation index indicates that the solution is undersaturated and the solid phase tends to dissolve, whereas a positive value indicates a clear tendency for precipitation. A value close to zero suggests that the solution is in equilibrium with the solid phase [30].

The removal capacity of zeolites was calculated by using Equation (1), while the removal degree (%*RD*) of copper ions from aqueous solutions was calculated by using Equation (2):

$$q_t = \frac{V(C_0 - C_t)}{m} \tag{1}$$

$$\%RD = \frac{(C_0 - C_t)}{C_0}\% \tag{2}$$

where q_t is the mass of removed Cu(II) ion per unit mass of zeolite (mg·g^{-1}); V is the volume of the aqueous phase (L); C_0 and C_t are the initial and final Cu(II) ion concentrations (mg·L^{-1}), respectively; and m is the mass of zeolite used (g).

The linearized kinetic models investigated in this study were the pseudo-first (Equation (3)) and pseudo-second-order models (Equation (4)) [31,32].

$$\log(q_e - q_t) = \log q_e - \frac{k_1 t}{2.303} \tag{3}$$

$$\frac{t}{q_t} = \frac{1}{k_2 q_e^2} + \frac{t}{q_e} \tag{4}$$

where q_e (mg·g^{-1}) is the amount of solute removed per unit mass of zeolite at equilibrium; and k_1 (min^{-1}) and k_2 (g·mg^{-1}·min^{-1}) are the apparent rate constants for pseudo-first-order and pseudo-second-order kinetics, respectively. Additionally, the intraparticle diffusion model was examined according to Equation (5) [33]:

$$q_t = K_p t^{0.5} + C \tag{5}$$

where K_p is the intraparticle diffusion rate constant (mg·g^{-1}·min$^{-0.5}$) and C (mg·g^{-1}) is a parameter related to the thickness of the boundary layer.

All experiments were carried out in duplicate and average values are given in the paper. It is important to note that all measured concentrations in similar tests were almost identical and the difference was ±2%.

2.4. Analytical Techniques

The chemical analysis of FA was performed using an X-ray fluorescence energy-dispersive spectrometer (Spectro XEPOS; Ametek Inc., Berwyn, PA, USA). X-ray diffraction (XRD) analyses were carried out with the use of Siemens D500 Diffractometer (Bruker D8-Focus powder diffractometer; Bruker, Karlsruhe, Germany), with nickel-filtered CuK radiation (λ = 1.5405 Å). The Brunauer-Emmett-Teller (BET) surface area of the synthetic zeolites was determined using a NOVA surface area analyzer (Quantachrome Nova 2200 analyzer; Anton Paar Quanta Tec Inc., Boynton Beach, FL, USA).

Prior to BET analysis, synthetic zeolites were pulverized and the particle size distribution was determined with the use of a Mastersizer S particle size analyzer (Malvern Instruments, Worcestershire, UK). The metal ion concentration in solution was determined with the use of inductively-coupled plasma mass spectrometry (ICP-MS) (Agilent Technologies 7500cx, Santa Clara, CA, USA).

A Fourier-transform infrared spectroscopy (FTIR) analysis was carried out on pellets produced after mixing a pulverized sample with KBr at a ratio of 1:100 *w/w*, using a Perkin Elmer Spectrum 1000 spectrometer (Perkin Elmer, Wellesley, MA, USA). A scanning electron microscopy (SEM) analysis was performed using a JEOL 6380LV scanning electron microscope (JEOL, Tokyo, Japan) equipped with an energy-dispersive X-ray spectroscopy (EDS) microanalysis system (INCA Energy 250; Oxford Instruments, Abington, UK) under low vacuum conditions (using pressure at 30 Pa, accelerating voltage at 20 kV, and working distance at 10–12 mm). The SEM/EDS examination was performed using a beam current and a beam size of 1 nA and 1 μm, respectively, on the sample. In each EDS quantification conducted, a dwell time of 30 s was applied.

X-Ray photoelectron spectroscopy (XPS), which enables elucidation of ion uptake and provides information on its chemical state [34–37], was carried out in an ultra-high vacuum chamber (UHV) equipped with an X-ray Al/Mg gun and a Phoibos 100 1D-DLD energy analyzer (Specs GmbH, Berlin, Germany). An unmonochromatized MgKα line at 1253.6 eV and an analyzer pass energy of 10 eV, giving a full width at half maximum (FWHM) of 0.85 eV for the Ag3d5/2 peak, was used in all XPS measurements. For spectra identification and fitting, the commercial software SpecsLab Prodigy (Specs GmbH, Berlin, Germany) was used. In this study, the atomic concentrations were calculated from the corresponding peak areas of Cu2p, Si2p, Al2p, and Na1s. Regarding Cu, peak fitting of the Cu2p spectrum revealed the presence of Cu ions on the chosen synthetic zeolite (ZFA1Na).

3. Results and Discussion

3.1. Raw Material and Zeolite Characterization

Table 1 shows the chemical composition of the FA used, while Figure 1 presents the mineralogical composition of the FA and the produced zeolites. It can be seen from Table 1 that the major oxides of FA were SiO_2, CaO, Al_2O_3, and Fe_2O_3 and since the content of SiO_2 + Al_2O_3 + Fe_2O_3 was ≥ 50% (i.e., 66.3%), the FA was classified as class C [38]. The SO_3 concentration (3.4% wt) and the loss on ignition (LOI; 3.9% wt) were lower than the maximum values of 5% wt and 6% wt, respectively, indicated for class C fly ashes. The Si/Al molar ratio in FA was 2.1.

Table 1. Chemical composition (wt %) of fly ash (FA).

Oxide	(wt %)	Oxide	(wt %)
SiO_2	40.4	MnO	0.08
CaO	16.4	P_2O_5	0.6
Al_2O_3	16.4	TiO_2	1.0
Fe_2O_3	9.5	SO_3	3.4
MgO	3.2	Cr_2O_3	0.04
K_2O	1.8	[a] LOI	3.9
Na_2O	3.3	Total	100.02

[a] LOI: Loss on ignition was determined after heating at 1050 °C for 2 h.

As shown in Figure 1, the main mineral phases present in FA were quartz and albite, while X- and A-type zeolites, sodium aluminum silicate hydrate, faujasite, and sodalite were clearly detected in ZFA1Na and ZFA1.5Na zeolites. Based on the XRD results, the ZFA1K and ZFA1.5K zeolites contained relatively low amount of F zeolite only. These results were in agreement with several earlier studies, which indicated that NaOH is a more efficient fusion agent compared with KOH for the production of zeolites [39–42].

Table 2 shows the particle size (in μm) and the BET surface area (in $m^2 \cdot g^{-1}$) of the produced synthetic zeolites. All zeolites had quite similar sizes (as indicated by the d_{50} values), which were

very fine and varied between 11 and 21 µm. The surface area of the K zeolites was almost double (~21.7 m$^2 \cdot$g^{-1}) compared with the surface area of the Na zeolites (~15.3 m$^2 \cdot$g^{-1}), while the surface area of the FA was 8.3 m$^2 \cdot$g^{-1}; the particle size of FA was <200 µm (d_{50} = 35 µm). Figure 2 shows the FTIR spectra of the Na and K zeolites as well as that of FA for comparison.
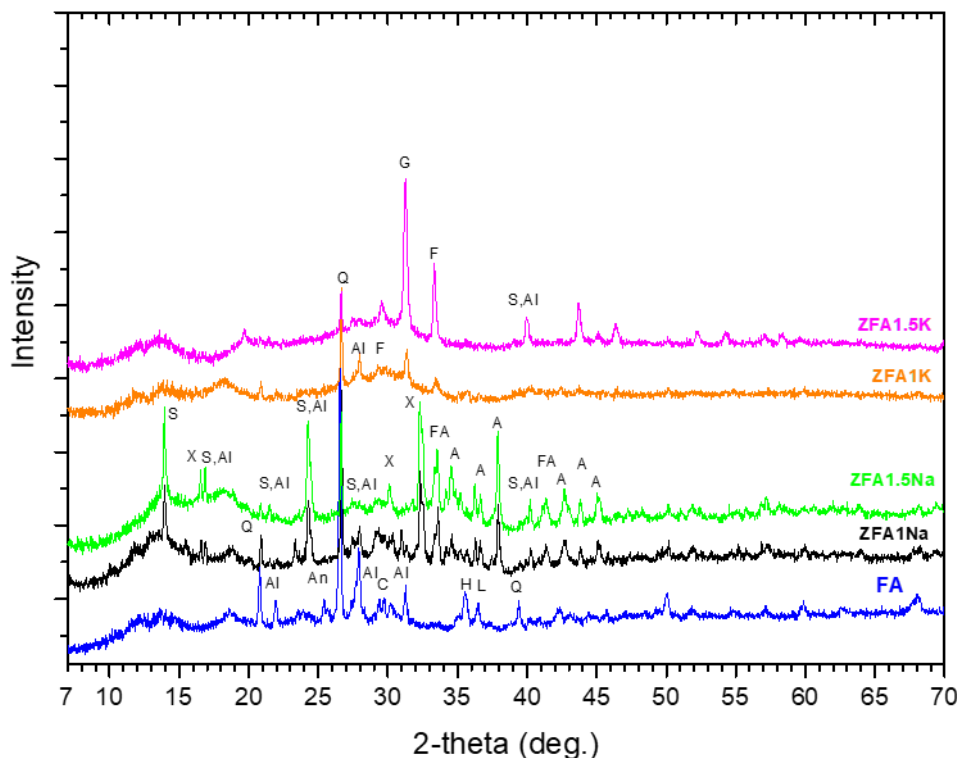

Figure 1. XRD patterns of FA, Na zeolites (ZFA1Na and ZFA1.5Na), and K zeolites (ZFA1K and ZFA1.5K). Q, quartz (SiO$_2$); Al, albite (NaAlSi$_3$O$_8$); G, gehlenite (Ca$_2$Al$_2$SiO$_7$); An, anhydrite (CaSO$_4$); H, hematite (Fe$_2$O$_3$); L, lime (CaO); C, calcite (CaCO$_3$); X, xeolite X (NaAlSi$_{1.23}$O$_{4.46} \cdot$3.07H$_2$O); A, zeolite A (NaAlSi$_{1.1}$O$_{4.2} \cdot$2.25H$_2$O); S,Al, sodium aluminum silicate hydrate (Na$_6$Al$_6$Si$_{10}$O$_{32} \cdot$12H$_2$O); S, sodalite (Na$_8$Al$_6$Si$_6$O$_{24}$Cl$_2$); FA, faujasite (Na$_2$Al$_2$Si$_{3.3}$O$_{8.8} \cdot$6.7H$_2$O); F, Linde F zeolite (KAlSiO$_4 \cdot$1.5H$_2$O).

Table 2. Particle size (µm) and surface area (m$^2 \cdot$g^{-1}) of the synthetic zeolites.

Zeolite Code	Particle Size (µm)		Specific Surface Area (m$^2 \cdot$g^{-1})
	Size	d_{50}	
ZFA1Na	<191	11.5	15.7
ZFA1.5Na	<118	17.4	14.8
ZFA1K	<132	11.3	21.9
ZFA1.5K	<223	20.9	21.5

The bands in the region 1090–990 and 750–550 cm^{-1} were common in all zeolites and indicated asymmetric and symmetric stretching vibration modes of Si-O-Si and Al-O-Si [43,44]. The asymmetric stretching vibration at 1090 cm^{-1} in FA became sharper and shifted to lower frequencies, i.e., 977 cm^{-1} and 998 cm^{-1}, in Na and K zeolites, respectively, indicating the formation of zeolitic products. The vibration bands at 874, 680, and 631 cm^{-1} were more intense in the produced zeolites compared with raw FA. The band at 1440 cm^{-1}, which was sharp for the zeolites, can be assigned to the stretching vibrations of O-C-O units. The peaks at 440 cm^{-1} can be attributed to bending vibration modes of Si-O-Si and O-Si-O in the FA and zeolite framework [45]. The broad band at 3500 cm^{-1} corresponded to stretching vibrations of adsorbed water and O-H groups. The band at 1630 cm^{-1} can be assigned to bending vibrations of O-H groups of water molecules [46].
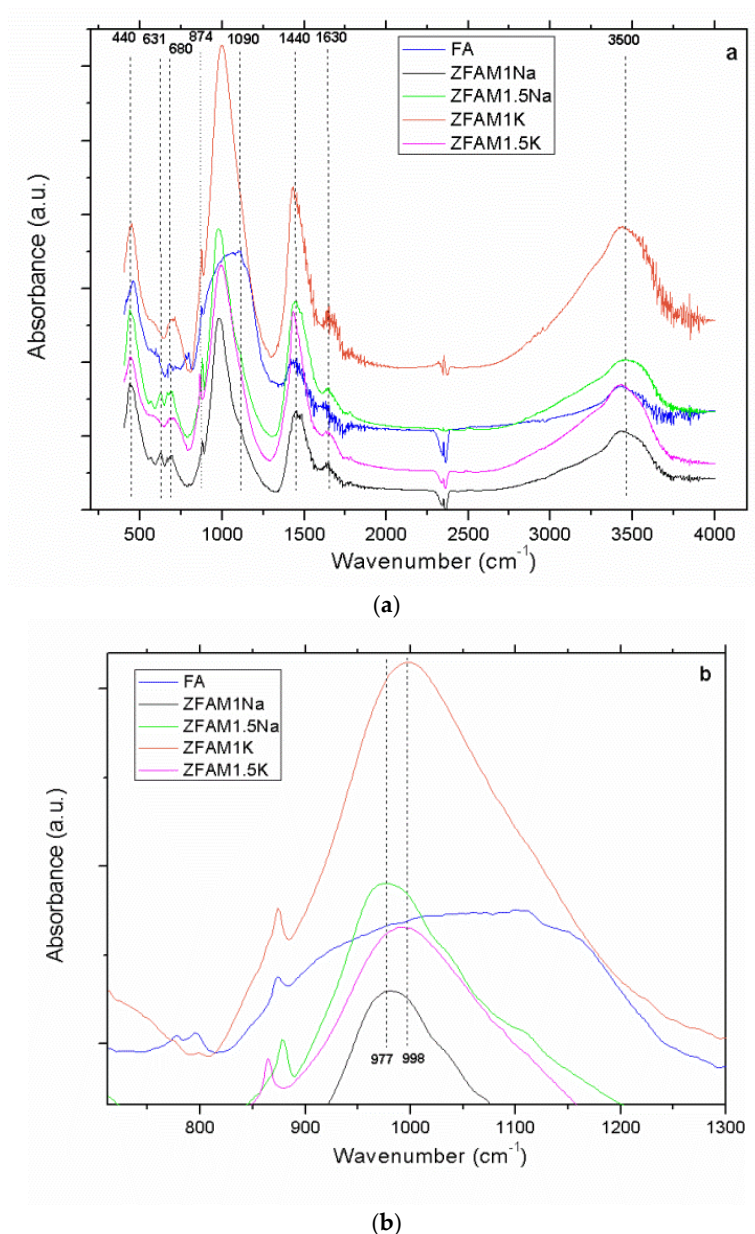
(**a**)

(**b**)

Figure 2. FTIR spectra (**a**) for all synthetic zeolites and raw FA; (**b**) zoomed area of the region between 800 and 1300 cm^{-1}.

3.2. Screening of Na and K Zeolites in Terms of Removal Efficiency

In order to screen the produced Na zeolites (ZFA1Na and ZFA1.5Na) and K zeolites (ZFA1K and ZFA1.5K) in terms of their removal efficiency, tests were carried out using a zeolite dosage of 0.5 g·L^{-1} and different initial Cu(II) concentrations, varying from 50 to 400 mg·L^{-1} (Figure 3).

Na zeolites showed higher removal efficiency compared with K zeolites, over the entire Cu(II) concentration range examined and especially at higher Cu(II) ion concentrations. For example, when the Cu(II) concentration was 200 mg·L^{-1}, the removal efficiency of ZFA1Na and ZFA1.5Na zeolites was 85% and 75%, respectively, while the removal efficiency of ZFA1K and ZFA1.5K zeolites was significantly lower, 50% and 55%, respectively. The removal efficiency of initial raw FA for the same Cu(II) ion concentration was less than 5% (data is not shown).

The higher removal efficiency of Na zeolites may be explained by the differences in their cation content and framework structure, compared with K zeolites. Sodium ions have higher hydrated radius (3.58 Å) compared with potassium ions (3.31 Å); thus, they are less strongly attached through

electrostatic interactions on the negatively charged surface of zeolites and can be more easily replaced by Cu(II) ions, as indicated in earlier studies [47,48]. In addition, it is known that the removal efficiency of zeolites depends on their effective pore size. As mentioned by Wang et al. [42], the pore sizes of zeolite A (4.2 Å), zeolite X (7.4 Å), and sodalite (2.3 Å), which are the main phases present in Na zeolites, are much larger than the unhydrated radius of Cu(II) ions (0.82 Å), thus favoring their removal; the hydrated radius of Cu(II) ions is 4.17 Å [31]. On the other hand, the pore size of F zeolite (2.6 Å), present in K zeolites, is also larger than the unhydrated radius of Cu(II) ions, but it is significantly smaller than the respective radii of the phases present in Na zeolites. Thus, higher removal efficiency of Na zeolites in comparison to K zeolites is anticipated. By taking into account these results, further removal studies were carried out with the use of ZFA1Na and ZFA1.5Na zeolites.
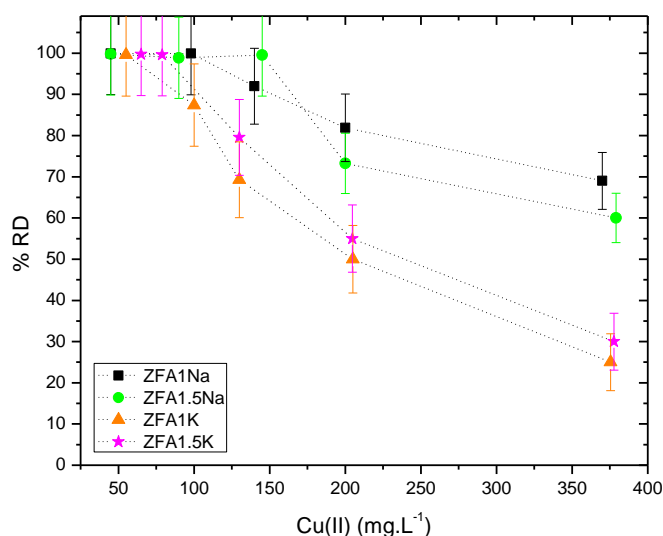

Figure 3. Removal efficiency of all zeolites (ZFA1Na, ZFA1.5Na, ZFA1K, and ZFA1.5K) for different initial Cu(II) ion concentrations (dosage, 0.5 g·L^{-1}; 25 °C).

3.3. Kinetic Studies

3.3.1. Effect of Initial Cu(II) Concentration

The removal efficiency of both the Na zeolites is shown in Figure 4.
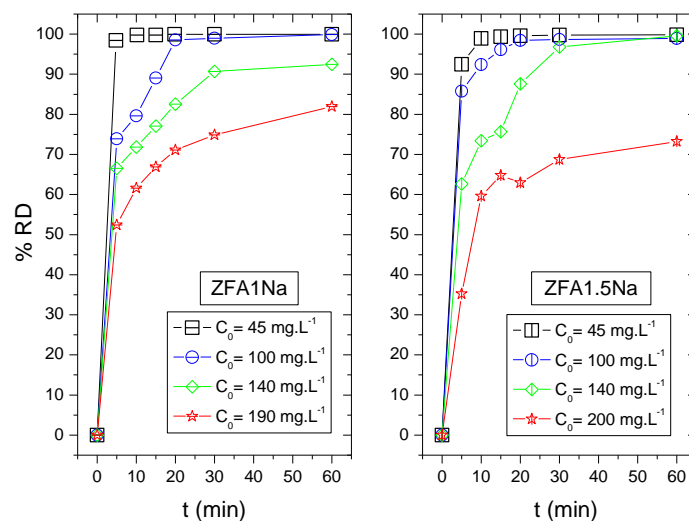

Figure 4. The removal degree (%RD) of ZFA1Na and ZFA1.5Na zeolites (dosage of 0.5 g·L^{-1}) as a function of the initial Cu(II) concentration (45–200 mg·L^{-1}).

These results showed that the removal of Cu(II) ions for both ZFA1Na and ZFA1.5Na zeolites was complete and reached equilibrium within 20 min for the initial Cu(II) ion concentrations 45 and 100 mg·L^{-1}. When the initial Cu(II) ion concentration increased to 140 mg·L^{-1}, equilibrium was reached in almost 30 min. Further increase in initial Cu(II) ion concentration to 200 mg·L^{-1} resulted in lower removal degree; however, this remained higher than 70% for both the zeolites, ZFA1Na and ZFA1.5Na (82% and 73%, respectively).

3.3.2. Effect of Zeolite Dosage

Given that in the previous series the efficiency of both the Na zeolites was quite similar, ZFA1Na zeolite was selected to assess the effect of dosage (0.3, 0.5, 1.0, and 1.5 g·L^{-1}) on Cu(II) ion uptake. The Cu(II) ion concentration selected was 140 mg·L^{-1} and the results are shown in Figure 5. It can be seen from the data that the increase of dosage resulted in an increase in the removal degree due to the increase in the number of available binding sites. At the lowest dosage used (0.3 g·L^{-1}), the removal efficiency of ZFA1Na was quite low, almost 50%, while complete copper removal was attained after just 10 min at dosages 1–1.5 g·L^{-1}.
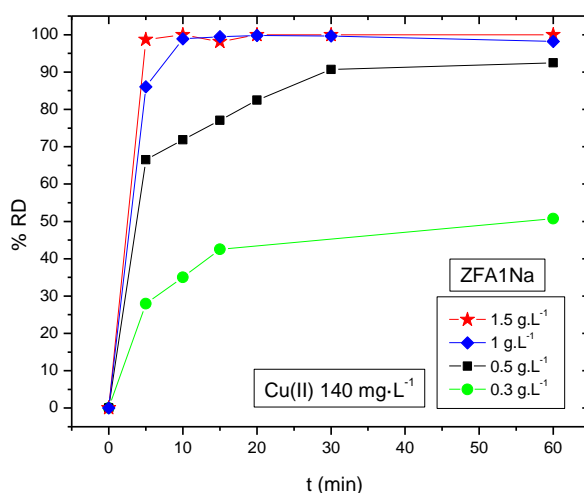

Figure 5. Effect of dosage (0.3–1.5 g·L^{-1}) on the removal efficiency of ZFA1Na zeolite (initial Cu(II) concentration of 140 mg·L^{-1}).

3.3.3. Evaluation of Kinetic Models

Kinetic modeling was carried out to define the rate-determining step during removal of Cu(II) ions, using the pseudo-first-order, pseudo-second-order, and intraparticle diffusion models; the dosage used was 0.5 g·L^{-1}. Figure 6 shows the evolution of the removal capacity with time, while Table 3 shows the respective apparent rate constants for each tested model.

Table 3. Kinetic parameters of copper removal from aqueous solutions onto synthetic zeolites.

[a] NZ	[b] Experimental	Pseudo-First-Order			Pseudo-Second-Order			Intraparticle Diffusion		
	$q_{e,exp}$ mg·g^{-1}	$q_{e,cal}$ mg·g^{-1}	k_1 min^{-1}	R^2	$q_{e,cal}$ mg·g^{-1}	k_2 g·mg^{-1}·min^{-1}	R^2	k_p mg·g^{-1}·min$^{-0.5}$	C mg·g^{-1}	R^2
Z1	93.49	10.72	0.260	0.721	93.54	0.3516	1.000	92.34	0.81	0.625
	196.41	158.74	0.160	0.905	201.21	0.0034	0.997	93.30	21.12	0.936
	258.69	204.87	0.117	0.930	265.96	0.0017	0.995	136.20	21.63	0.990
	309.70	202.44	0.075	0.878	318.47	0.0011	0.994	145.95	26.33	0.951
Z1.5	90.08	31.43	0.260	0.918	90.33	0.0756	0.999	3.91	75.38	0.698
	176.54	95.52	0.201	0.929	177.94	0.0122	0.999	10.14	131.5	0.975
	290.79	255.81	0.108	0.946	302.11	0.0011	0.991	23.75	132.7	0.838
	294.01	206.82	0.089	0.847	305.81	0.0011	0.991	29.03	135.9	0.722

[a] NZ, Na zeolites; Z1 and Z1.5, ZFA1Na and ZFA1.5Na, respectively; [b] dosage, 0.5 g·L^{-1}; 25 °C; stirring speed, 600 rpm; time, 60 min.
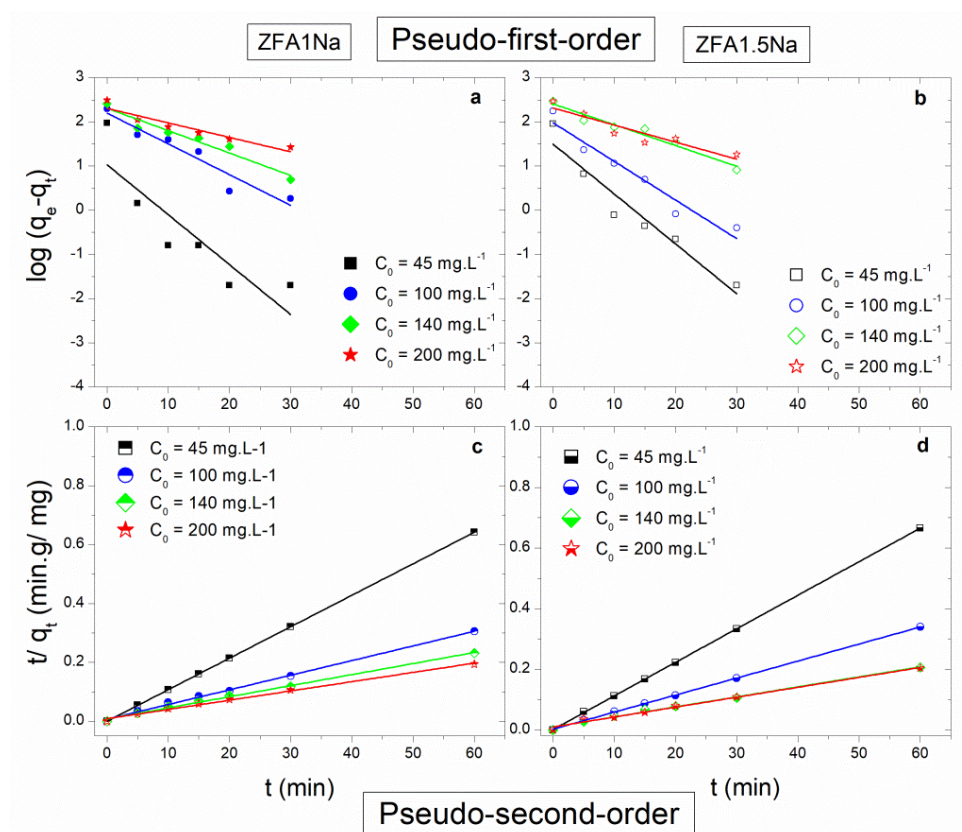
Figure 6. Pseudo-first-order (**a**,**b**) and pseudo-second-order (**c**,**d**) removal of Cu onto ZFA1Na and ZFA1.5Na zeolites (dosage 0.5 g·L^{-1}, Cu concentration 45–200 mg L^{-1}).

It was seen from the data that the pseudo-second-order model fits (R^2 values, 0.991–1) the experimental data very well for both the zeolites used, indicating that the reaction rate depended on the number of available active sites on the surface [32,49,50]. For the initial Cu(II) ion concentrations of 45 and 100 mg·L^{-1}, the removal capacity of ZFA1Na was 93 and 196 mg·g^{-1}, respectively; this capacity was significantly higher compared with the capacity (40–70 mg·g^{-1}) calculated in an earlier study in which the removal of multiple metal ions, namely, Co(II), Cr(III), Ni(II), Zn(II), and Cu(II), was investigated with the use of zeolites [29]. The calculated removal capacity, $q_{e,cal}$ agreed well with the experimental removal capacity, $q_{e,exp}$; the maximum difference was 4%. The apparent rate constant, k_2, varied for different initial concentrations of Cu(II) ions, especially for the smaller ones.

It was noted that the removal capacity ($q_{e,cal}$) increased with an increase in the initial copper concentrations and seemed to stabilize at the higher initial Cu(II) ion concentrations tested, 140 and 200 mg L^{-1}. These results were consistent with previous studies [51,52]. The kinetics of Cu(II) removal on coal ash-derived zeolite was also described by the pseudo-second-order model [53] and showed higher equilibrium time (>50 h at 30 and 40 °C) compared with the present study (<1 h).

The pseudo-second-order kinetic model is based on the assumption that the chemisorption is the rate-determining step [54]. However, the removal mechanism cannot be based on simple fitting of the pseudo-second-order model [55]. Both pseudo-first-order and pseudo-second-order models did not explain the diffusion of the solute into the material; therefore, before any conclusions were drawn about the mechanism, the intraparticle diffusion model was also investigated. According to this model, the nature of the rate-controlling step is predicted by taking into account surface and/or pore diffusion. The resulting straight lines did not cross the origin (Figure 7) and therefore, intraparticle diffusion was not the only rate-limiting step. However, the nonlinearity of copper data indicated that more than one process was involved in copper removal. In particular, the first sharp relation (first linear fit) was attributed to copper diffusion from the solution to the external surface of synthetic zeolites

(external diffusion), whereas the second relation (second linear fit) revealed progressive ion diffusion inside the pores (intraparticle diffusion). The kinetic data indicated that the mechanism of copper ion removal from aqueous solutions was complex and probably involved a combination of chemisorption and intraparticle diffusion through the surface/pores of synthetic zeolites. This finding was in line with previous kinetic studies involving heavy metal uptake from synthetic zeolites [56,57].
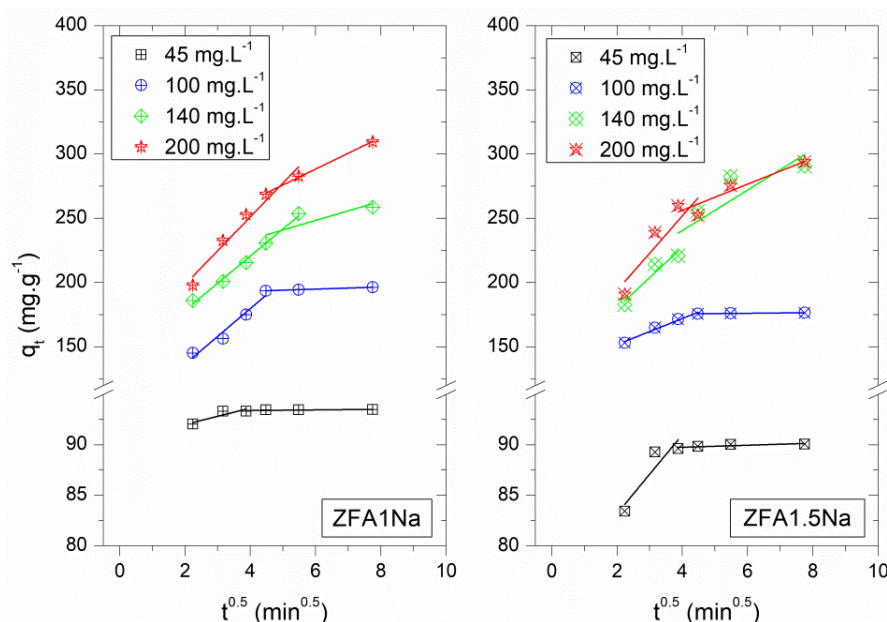

Figure 7. Intraparticle diffusion model for copper removal onto ZFA1Na and ZFA1.5Na zeolites.

Table 4 presents the results of previous studies pertinent to the removal of Cu(II) ions on zeolites produced from lignite fly ash and other materials and compares them with the results of the present study. The low removal capacity of natural zeolite (1 mg·g^{-1} for Cu(II)) was evaluated for Cu(II) aqueous solutions when a very high dosage (37 g·L^{-1}) was used [58]. The removal capacity of fly ash-derived zeolites, namely, zeolite types A and X and coal ash-based zeolites [31,42], were lower compared with that in our study even when a high dosage (5 g·L^{-1}) was used. Pyrolyzed pistachio shells (biochar) can also be effectively used for the removal of Cu(II) [57]. In the present study, the removal capacity of raw FA was also determined and found to be 38 mg·g^{-1}. However, the removal capacity of ZFA1Na was higher (q_e, ~310 mg·g^{-1}) compared with that observed for all other studies when a low dosage (0.5 g·L^{-1}) was used.

Table 4. Data on Cu(II) and Zn(II) (initial concentration values) removal by zeolite-type materials.

Materials Used for Copper Removal	Cu(II) Concentration mg·L^{-1}	pH	T °C	Time h	Dosage g·L^{-1}	Removal Capacity mg·g^{-1}	Removal Degree %	Reference
Natural zeolite (clinoptilolite)	20	3.5	22	6	37	0.54	98	[58]
Zeolite A	200	3	25	4	5	38		[42]
Zeolite X	200	3	25	4	5	29		
Zeolite 4A (from coal fly ash)	100	3–4	25	4	1	20–70	20–80	[31]
Pistachio shell biochar	150	7.15 *	25	24	10	9.5	63	[59]
ZFA1Na	200	5.5	25	1	0.5	310	80	Present study

* The pH was measured in the aqueous solution containing biochar produced at 550 °C.

3.4. Morphology and Composition Analysis of Zeolites

Based on the SEM/EDS analysis, the morphology of selected synthetic zeolites (ZFA1Na and ZFA1K) prior to and after copper removal is shown in Figure 8a,c. Due to their inherent characteristics, raw FA mostly presented a smooth spherical surface consisting of solid ash particles and cenospheres

(image not shown). On the other hand, both zeolite surfaces turned from smooth in the FA to rugged, due to the formation of new zeolite crystal clusters as a result of alkaline fusion. The synthetic zeolite ZFA1Na presented an angular-like structure consisting of cubic crystals with an almost constant size (~15 μm), typical for A-type zeolite [60], which was confirmed by XRD results. However, the synthetic zeolite ZFA1K exhibited higher heterogeneity both in size and shape compared with ZFA1Na. In this case, prism-like clusters of varying sizes (up to 22 μm) and irregular shapes were formed onto the synthetic zeolite particles, typical for Linde F-type zeolite [40] and in accordance with XRD results.
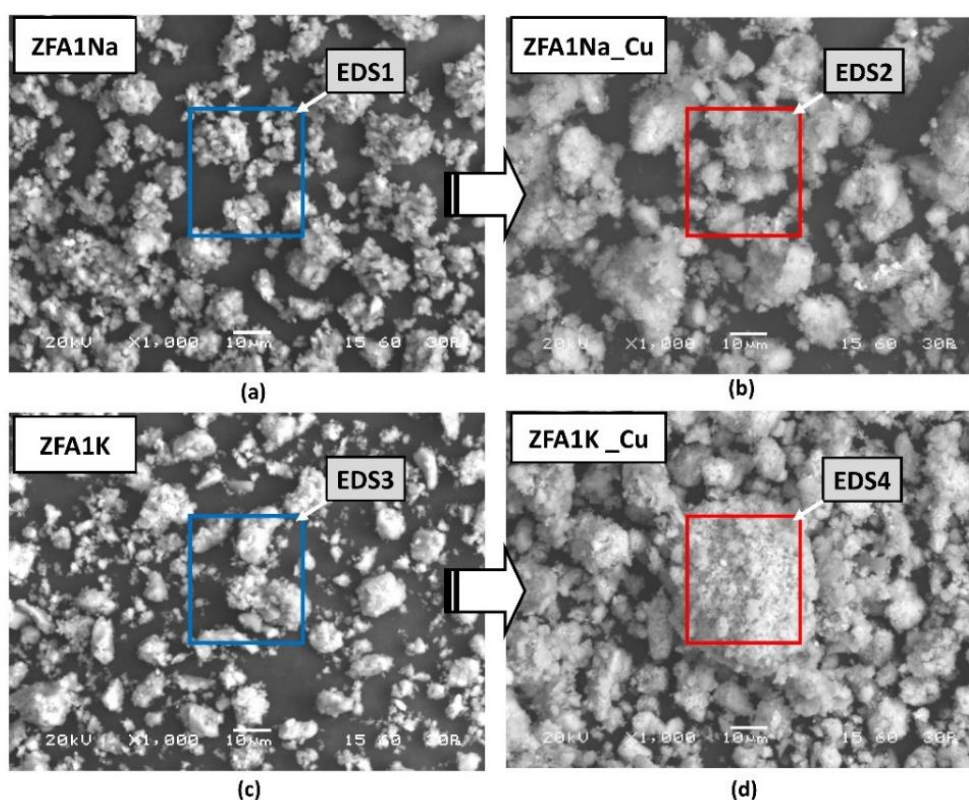

Figure 8. Comparison of morphology obtained for synthetic zeolites ZFA1Na and ZFA1K based on SEM/EDS analyses prior to ((**a**) ZFA1Na and (**c**) and ZFA1K) and after removal ((**b**) ZFA1Na_Cu and (**d**) ZFA1K_Cu) of Cu(II) ions. Concentration, 200 mg·L^{-1}; zeolite dosage, 0.5 g·L^{-1}. EDS analyses were performed on the square highlighted regions (1–4).

After copper removal, the morphology of ZFA1Na_Cu (Figure 8b) and ZFA1K_Cu (Figure 8d) changed significantly and exhibited a more crystalline structure with greater degree of agglomeration and uniformity. EDS analyses carried out on representative regions (blue squares) of the zeolites ZFA1Na and ZFA1K showed that their semi-quantitative elemental composition corresponded to Ca, Al, Fe, and Si along with the higher intensity of Na and/or K, depending on the fluxing agents used, i.e., NaOH or KOH (spectra a and c of Figure 9, respectively). After removal, EDS spectra corresponding to red square regions (EDS2 and EDS4) clearly confirmed the presence of copper on the surfaces of the synthetic zeolites (ZFA1Na and ZFA1K), as shown in spectra b and d of Figure 9, respectively.

Copper was detected by SEM/EDS analyses on both the synthetic zeolites, ZFA1Na_Cu and ZFA1K_Cu, revealing that Cu(II) ions were removed from aqueous solutions. In both the cases, the disappearance of Ca, Mg, K, and Na may indicate their contribution to ion-exchange reactions involving Cu(II) ions [61]. Cations within the zeolite channels are free to move and are prone to diffuse into the bulk solution phase during experiments [62]. On the other hand, the appearance of Cl on the surface of both the zeolites (atomic percentage (at. %), 7–10) was the result of the use of 0.1 M NaCl for the preparation of aqueous solutions with a constant ionic strength.
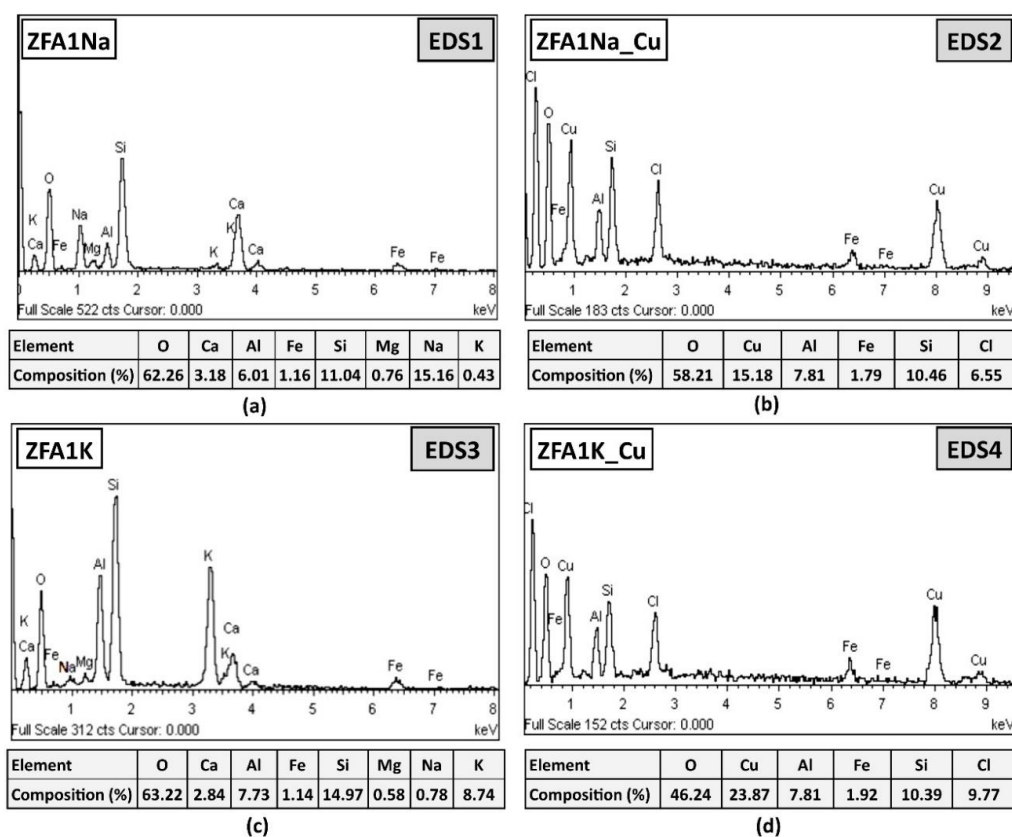
Figure 9. EDS spectra and elemental composition in terms of atomic percentage (at. %) of the synthetic zeolites prior to ((**a**) ZFA1Na and (**c**) and ZFA1K) and after removal ((**b**) ZFA1Na_Cu and (**d**) ZFA1K_Cu) of Cu(II) ions, respectively (shown as square regions in Figure 3). Initial Cu ion concentration, 200 mg·L^{-1}; zeolite dosage, 0.5 g·L^{-1}.

3.5. Copper Chemical State by XPS Analysis

The chemical state of Cu and the relative atomic concentration of the zeolite's surface was investigated by means of XPS spectroscopy. XRS was performed in the synthetic zeolite before (ZFA1Na) and after (ZFA1Na_Cu) copper removal (initial copper concentration, 200 mg·L^{-1}; zeolite dosage, 0.5 g·L^{-1}). In the XPS survey scans (Figure 10) of the synthetic zeolite before and after copper removal, Al, Si, O, Na, and Cl peaks were present on both the surfaces, whereas intense Na peaks were present on the ZFA1Na surface and Cu prevailed on ZFA1Na_Cu. Moreover, Ca peaks were present in the ZFA1Na sample, whereas in the ZFA1Na_Cu sample, the peak overlapped with the CuLVV (L-shell valence valence) Auger peaks. The detailed Cu2p, Si2p, and the combined Al2p-Cu3p XPS core level spectra of both samples are provided as Supplementary Material (Figure S2).

From the peak area of Cu2p3/2, Si2p, Al2p, Na1s, and Cl2p, the atomic concentration (At, %) can be calculated at appointed binding energies (Table 5). The binding energy of Cu2p3/2 of ZFA1Na_Cu sample at 934.3 eV and a high copper atomic concentration (26.8%) was measured for the synthetic zeolite after copper removal. The Cu2p peak shape with the intense satellites proved that Cu(II) ions were present on the synthetic surface (within 10 nm depth according to XPS analysis limitations) in small cages as well as in open channels of the zeolite.

In order to identify the chemical state of Cu, the CuLVV spectrum (X-ray-induced Auger electron spectroscopy) was recorded (not shown); and the Cu-modified Auger parameter, α, (derived from the sum of the Cu2p3/2 binding energy and the CuL3VV kinetic energy) was 1851.6 eV. Chen et al. [63] suggested the presence of Cu(II) ion species as a CuO cluster at 933.7 eV inside the zeolite pore structure. They supported that, due to low hydration energy, Cu ions can lose part of their water of hydration. The partially hydrated Cu ions are small enough to enter the zeolite channels, giving rise to

Cu-distribution ions through the synthetic zeolite surface. According to Biesinger et al. [64], the binding energy of Cu 2p3/2 for CuO assigned to Cu(II) species was at 933.6 eV, whereas for Cu(OH)$_2$, it was at 934.8 eV. On the contrary, the Auger parameter was 1851.4 ± 0.1 eV for both CuO and Cu(OH)$_2$. Therefore, our results indicated that CuO and/or Cu(OH)$_2$ were present in the zeolite. In addition, Cl2p binding energy region showed a characteristic Cl2p3/2 peak at 198.2 eV. This may be assigned to chlorine atoms as Cu-Cl, forming low amounts of atacamite [65].

Figure 10. XPS survey scans of ZFA1Na and ZFA1Na_Cu samples.

Table 5. Surface atomic concentrations of main elements in zeolite before (ZFA1Na) and after copper removal (ZFA1Na_Cu). Comparison of surface atomic ratios derived from XPS with SEM/EDS.

		Sample No.	
		[a] **ZFA1Na**	**ZFA1Na_Cu**
Surface analysis (XPS)			
Cu2p3/2	[b] Eb (eV)	n.a.	934.3
	[c] At (%)	n.a.	26.8 ± 0.3
Si2p	Eb (eV)	102.2	102.0
	At (%)	19.6 ± 0.3	20.6 ± 0.3
Al2p	Eb (eV)	73.9	73.7
	At (%)	13.8 ± 0.5	20.1 ± 0.7
Na1s	Eb (eV)	1072.2	1072.5
	At (%)	61.0 ± 0.3	19.2 ± 0.3
Cl2p	Eb (eV)	198.2	198.2
	At (%)	5.5 ± 0.01	13.1 ± 0.3
Cu/Si		n.a.	1.3
Si/Al		1.4	1.0
Na/Si		3.1	0.9
Cl/Si		0.3	0.6
Bulk analysis (SEM/EDS)			
Cu/Si		n.a.	1.5
Si/Al		1.8	1.3

[a] Abbreviations: Fly ash-derived zeolite (ZFA1Na) and after removal of copper solution (ZFA1Na_Cu); initial Cu ion concentration, 200 mg·L^{-1}; dosage, 0.5 g.L^{-1}; NaCl, 0.1 M. [b] Eb, binding energy (eV); [c] (At, %) atomic concentration; n.a., not applicable.

The atomic concentration of Si on the zeolite surface was relatively increased compared with that of the synthetic zeolite and the atomic concentration of Al was increased from 13.8% to 20.1% with a broader spectrum after copper removal. A decrease in Na loading from 61.0% to 19.2% was defined, implying that Na may be involved as an exchangeable cation in the uptake of Cu. Despite the presence of NaCl in solution, the XPS analysis revealed that potentially available Na ions from NaCl did not interact with the surface during the process. However, Na and Cl ions initially present in the synthetic zeolite may contribute to the copper removal process.

The comparison of Cu/Si, Si/Al and Na/Si atomic ratios on the surface for the synthetic zeolite (before and after copper removal) was calculated. The Cu/Si ratio increased, indicating the presence of copper on the synthetic zeolite surface after copper removal from aqueous solutions. Both Si/Al and Na/Si atomic ratios decreased from 1.4 to 1.0 and from 3.1 to 0.9, respectively. The Cu/Si ratio after EDS analysis was higher compared with that after XPS analysis, due to higher copper content in the bulk compared with surface analysis (XPS). XPS measurements are bound to the limited penetration depth of a few nanometers (i.e., <10 nm) from the surface as well as to the dependence on the distribution of copper species. Therefore, copper content measured by XPS can become an indicator to which extent Cu is inserted into the zeolitic channels when comparing the results with the EDS measurements that probe the bulk composition of the samples. However, XPS analysis data correlated well with that of SEM/EDS analyses considering Si/Al atomic ratios. The coincidence of Si/Al ratio measurements from XPS and bulk analysis was often determined [66].

No shift in binding energy of appointed components was monitored, thus no new chemical bonding was observed. Differences in Si/Al, Na/Si, and Cu/Si ratios may reveal the migration of ions from the bulk to the surface [66], thus indicating diffusion as a possible removal mechanism among aqueous copper ions and Na ions initially present in synthetic zeolites. The XPS spectra analysis may explain the removal mechanism in cases where various interactions between surface active sites (functional groups) and metal ions occur [67]. Kim et al. [35] studied iron-incorporated A-type zeolite, revealing a decrease in Si/Al and Na/Si ratios after XPS analysis. A surface composition analysis of natural zeolites before and after heavy metal uptake showed a decrease in Na/Si ratio, whereas the Si/Al ratio was constant [34]. In this study, the Si/Al atomic ratio for the synthetic zeolite after copper removal was close to 1, demonstrating A-type zeolite. Zeolite A has the framework composition with a high Al content and an Si/Al molar ratio of almost 1. In tetrahedral aluminosilicate frameworks, this is the highest Al content [68]. In zeolite A, the Al-framework is balanced by the maximum number of cation-exchange sites; it has a high cation content and superior exchange capacity and potentially may have applications for ion-exchange in industrial processes [69].

4. Conclusions

Greek lignite fly ash was efficiently converted into zeolites through alkaline fusion with the use of NaOH and KOH. Mineralogical analyses revealed the presence of zeolite A, zeolite X, and sodalite on the zeolites obtained after NaOH fusion and Linde F-type zeolite after KOH fusion. Screening tests involving the removal of Cu(II) ions indicated that Na zeolites exhibited higher copper removal efficiency compared with K zeolites.

The removal capacity of Na zeolites for Cu(II) ions depended mainly on the initial Cu(II) ion concentration present in the aqueous solution. The removal capacity obtained for Cu(II) ions in the present study was very high and reached 310 and 294 mg·g^{-1} for ZFA1Na and ZFA1.5Na zeolites, respectively. The removal kinetics were quite fast within the first 30 min, indicating that ~70% of Cu(II) ions, at the initial metal concentration of 200 mg·L^{-1}, were removed from the solution. The pseudo-second-order kinetic model fit the experimental data very well. SEM/EDS analyses proved the presence of copper in the zeolitic framework including open channels and the presence of Cu(II) oxidation state possibly due to the formation of CuO and/or Cu-Cl according to XPS analysis.

In conclusion, the present study proved that synthetic zeolites can be produced from lignite fly ash and can be used as efficient materials for the decontamination of industrial wastewaters containing

high amounts of Cu(II) ions. This approach can result in the valorization of industrial wastes and the elimination of environmental problems caused by their improper disposal mainly at lignite mining centers and combustion stations.

References

1. Market Report Series: Coal 2019. Analysis and Forecasts to 2024. Available online: https://www.iea.org/reports/coal-2019 (accessed on 17 September 2020).

2. Belviso, C. State-of-the-art applications of fly ash from coal and biomass: A focus on zeolite synthesis processes and issues. *Prog. Energy Combust. Sci.* **2018**, *65*, 109–135. [CrossRef]

3. Zaravelis, F.; Theodorakis, N.; Triantafyllou, A.; Stivanakis, V. Fly ash of Megalopolis and ferroalumina in the production of building materials. *Mater. Today Proc.* **2018**, *5*, 27434–27440. [CrossRef]

4. Jambhulkar, H.P.; Shaikh, S.M.S.; Kumar, M.S. Fly ash toxicity, emerging issues and possible implications for its exploitation in agriculture; Indian scenario: A review. *Chemosphere* **2018**, *213*, 333–344. [CrossRef]

5. Chousidis, N.; Rakanta, E.; Ioannou, I.; Batis, G. Mechanical properties and durability performance of reinforced concrete containing fly ash. *Constr. Build. Mater.* **2015**, *101*, 810–817. [CrossRef]

6. Savvilotidou, V.; Kritikaki, A.; Stratakis, A.; Komnitsas, K.; Gidarakos, E. Energy efficient production of glass-ceramics using photovoltaic (P/V) glass and lignite fly ash. *Waste Manag.* **2019**, *90*, 46–58. [CrossRef]

7. Komnitsas, K.; Zaharaki, D.; Perdikatsis, V. Geopolymerisation of low calcium ferronickel slags. *J. Mater. Sci.* **2006**, *42*, 3073–3082. [CrossRef]

8. Toniolo, N.; Boccaccini, A.R. Fly ash-based geopolymers containing added silicate waste. A review. *Ceram. Int.* **2017**, *43*, 14545–14551. [CrossRef]

9. Ram, L.; Masto, R. Fly ash for soil amelioration: A review on the influence of ash blending with inorganic and organic amendments. *Earth Sci.Rev.* **2014**, *128*, 52–74. [CrossRef]

10. Volli, V.; Purkait, M.K.; Shu, C.-M. Preparation and characterization of animal bone powder impregnated fly ash catalyst for transesterification. *Sci. Total. Environ.* **2019**, *669*, 314–321. [CrossRef]

11. Mushtaq, F.; Zahid, M.; Bhatti, I.A.; Nasir, S.; Hussain, T. Possible applications of coal fly ash in wastewater treatment. *J. Environ. Manag.* **2019**, *240*, 27–46. [CrossRef]

12. Chen, L.; Wang, L.; Cho, D.-W.; Tsang, D.C.; Tong, L.; Zhou, Y.; Yang, J.; Hu, Q.; Poon, C.S. Sustainable stabilization/solidification of municipal solid waste incinerator fly ash by incorporation of green materials. *J. Clean. Prod.* **2019**, *222*, 335–343. [CrossRef]

13. Chaikittisilp, W.; Okubo, T. Zeolite and Zeolite-Like Materials. *Handb. Solid State Chem.* **2017**, *7*, 97–119. [CrossRef]

14. Koshy, N.; Singh, D.N. Fly ash zeolites for water treatment applications. *J. Environ. Chem. Eng.* **2016**, *4*, 1460–1472. [CrossRef]

15. Belviso, C.; Cavalcante, F.; Fiore, S. Synthesis of zeolite from Italian coal fly ash: Differences in crystallization temperature using seawater instead of distilled water. *Waste Manag.* **2010**, *30*, 839–847. [CrossRef]

16. Franus, M.; Wdowin, M.; Bandura, L.; Franus, W. Removal of environmental pollutions using zeolites from fly ash: A review. *Fres. Environ. Bull.* **2015**, *24*, 854–866.

17. Asl, S.M.H.; Javadian, H.; Khavarpour, M.; Belviso, C.; Taghavi, M.; Maghsudi, M. Porous adsorbents derived from coal fly ash as cost-effective and environmentally-friendly sources of aluminosilicate for sequestration of aqueous and gaseous pollutants: A review. *J. Clean. Prod.* **2019**, *208*, 1131–1147. [CrossRef]

18. Itskos, G.; Koutsianos, A.; Koukouzas, N.; Vasilatos, C. Zeolite development from fly ash and utilization in lignite mine-water treatment. *Int. J. Miner. Process.* **2015**, *139*, 43–50. [CrossRef]

19. Moutsatsou, A.; Stamatakis, M.; Hatzitzotzia, K.; Protonotarios, V. The utilization of Ca-rich and Ca–Si-rich fly ashes in zeolites production. *Fuel* **2006**, *85*, 657–663. [CrossRef]

20. Ramírez, H.; Núñez, M.M.G.; Bogoya, A.B.; Gomez, D.F.B.; Ramos, C.; Di Luca, C.; Inchaurrondo, N.; Haure, P. Synthesis of coal fly ash zeolite for the catalytic wet peroxide oxidation of Orange II. *Environ. Sci. Pollut. Res.* **2018**, *26*, 4277–4287. [CrossRef]

21. Gupta, S.S.; Bhattacharyya, K.G. Adsorption of metal ions by clays and inorganic solids. *RSC Adv.* **2014**, *4*, 28537–28586. [CrossRef]

22. Megías-Sayago, C.; Lara-Ibeas, I.; Wang, Q.; Le Calvé, S.; Louis, B. Volatile organic compounds (VOCs) removal capacity of ZSM-5 zeolite adsorbents for near real-time BTEX detection. *J. Environ. Chem. Eng.* **2020**, *8*, 103724. [CrossRef]

23. Maiti, S.; Raj, H.; Bisht, R.; Minocha, A.K.; Panigrahi, S.K.; Alexander, S.J.; Singh, M. X—Ray photoelectron spectroscopy study on adsorption property of harmful air pollutants on zeolite prepared from fly ash. *Mater. Res. Express* **2018**, *5*, 085507. [CrossRef]

24. Tolentino, C.M.C.; De Luna, M.D.G.; Futalan, C.M.; Choi, A.E.S.; Manegdeg, F.G.; Grisdanurak, N. Influence of hydrocarbons on hydrogen chloride removal from refinery off-gas by zeolite NaY derived from rice husks. *Sci. Total. Environ.* **2020**, *728*, 138782. [CrossRef]

25. Lahori, A.H.; Mierzwa-Hersztek, M.; Demiraj, E.; Sajjad, R.U.; Ali, I.; Shehnaz, H.; Aziz, A.; Zuberi, M.H.; Pirzada, A.M.; Hassan, K.; et al. Direct and residual impacts of zeolite on the remediation of harmful elements in multiple contaminated soils using cabbage in rotation with corn. *Chemosphere* **2020**, *250*, 126317. [CrossRef]

26. Moraetis, D.; Papagiannidou, S.; Pratikakis, A.; Pentari, D.; Komnitsas, K. Effect of zeolite application on potassium release in sandy soils amended with municipal compost. *Desalin. Water Treat.* **2015**, *57*, 1–12. [CrossRef]

27. Wen, J.; Yi, Y.; Zeng, G. Effects of modified zeolite on the removal and stabilization of heavy metals in contaminated lake sediment using BCR sequential extraction. *J. Environ. Manag.* **2016**, *178*, 63–69. [CrossRef]

28. Zhao, H.; Huang, X.; Liu, F.; Hu, X.; Zhao, X.; Wang, L.; Gao, P.; Ji, P. A two-year field study of using a new material for remediation of cadmium contaminated paddy soil. *Environ. Pollut.* **2020**, *263*, 114614. [CrossRef]

29. Parkhurst, D.L.; Appelo, C. Description of Input and Examples for PHREEQC Version 3: A Computer Program for Speciation, Batch-Reaction, One-Dimensional Transport, and Inverse Geochemical Calculations. In *Techniques and Methods*; book 6; U.S. Geological Survey: Reston, VA, USA, 2013; 497p.

30. Komnitsas, K.; Bartzas, G.; Paspaliaris, I. Modeling of Reaction Front Progress in Fly Ash Permeable Reactive Barriers. *Environ. Forensics* **2006**, *7*, 219–231. [CrossRef]

31. Hui, K.S.; Chao, C.; Kot, S.; Chao, C.Y.H. Removal of mixed heavy metal ions in wastewater by zeolite 4A and residual products from recycled coal fly ash. *J. Hazard. Mater.* **2005**, *127*, 89–101. [CrossRef]

32. Komnitsas, K.; Zaharaki, D.; Bartzas, G.; Alevizos, G. Adsorption of Scandium and Neodymium on Biochar Derived after Low-Temperature Pyrolysis of Sawdust. *Minerals* **2017**, *7*, 200. [CrossRef]

33. Mthombeni, N.H.; Onyango, M.S.; Aoyi, O. Adsorption of hexavalent chromium onto magnetic natural zeolite-polymer composite. *J. Taiwan Inst. Chem. Eng.* **2015**, *50*, 242–251. [CrossRef]

34. Yuan, G.; Seyama, H.; Soma, M.; Theng, B.K.G.; Tanaka, A. Adsorption of some heavy metals by natural zeolites: XPS and batch studies. *J. Environ. Sci. Health Part A* **1999**, *34*, 625–648. [CrossRef]

35. Kim, K.S.; Park, J.O.; Nam, S.C. Synthesis of Iron-loaded Zeolites for Removal of Ammonium and Phosphate from Aqueous Solutions. *Environ. Eng. Res.* **2013**, *18*, 267–276. [CrossRef]

36. Gao, Y.; Ru, Y.; Zhou, L.; Wang, X.; Wang, J. Preparation and Characterization of Chitosan-Zeolite Molecular Sieve Composite for Ammonia and Nitrate Removal. *Adv. Compos. Lett.* **2018**, *27*, 185–192. [CrossRef]

37. Sygellou, L. An in-situ photoelectron spectroscopy study of the thermal processing of ammonium tetrathiomolybdate, (NH4)2MoS4, precursor. *Appl. Surf. Sci.* **2019**, *476*, 1079–1085. [CrossRef]

38. ASTM C618: Standard Specification for Coal Fly Ash and Raw or Calcined Natural Pozzolan for Use in Concrete. Designation: C618−12a. Available online: http://materialstandard.com/wp-content/uploads/2019/08/C618-12a.pdf. (accessed on 23 September 2020).

39. Medina, A.R.; Gamero, P.M.; Almanz, J.M.R.; Cortés, D.A.H.; Vargas, G. Study of the zeolitization process of fly ash using an orthogonal array of taguchi experimental design. *J. Chil. Chem. Soc.* **2009**, *54*, 244–251. [CrossRef]

40. Miyaji, F.; Murakami, T.; Suyama, Y. Formation of linde F zeolite by KOH treatment of coal fly ash. *J. Ceram. Soc. Jpn.* **2009**, *117*, 619–622. [CrossRef]

41. Querol, X.; Moreno, N.; Umaña, J.; Alastuey, A.; Hernández, E.; Lopez-Soler, A.; Plana, F. Synthesis of zeolites from coal fly ash: An overview. *Int. J. Coal Geol.* **2002**, *50*, 413–423. [CrossRef]

42. Wang, C.; Li, J.; Sun, X.; Wang, L.; Sun, X. Evaluation of zeolites synthesized from fly ash as potential adsorbents for wastewater containing heavy metals. *J. Environ. Sci.* **2009**, *21*, 127–136. [CrossRef]

43. Mainganye, D.; Ojumu, T.; Petrik, L. Synthesis of Zeolites Na-P1 from South African Coal Fly Ash: Effect of Impeller Design and Agitation. *Materials* **2013**, *6*, 2074–2089. [CrossRef]

44. Wang, P.; Sun, Q.; Zhang, Y.; Cao, J. Synthesis of Zeolite 4A from Kaolin and Its Adsorption Equilibrium of Carbon Dioxide. *Materials* **2019**, *12*, 1536. [CrossRef] [PubMed]

45. Azizli, K.; Rahi, R.A.; Man, Z.; Rahmiati, T.; Nuruddin, M. Effect of Sodium Hydroxide Concentration on the Mechanical Property of Non Sodium Silicate Fly Ash Based Geopolymer. *J. Appl. Sci.* **2014**, *14*, 3381–3384. [CrossRef]

46. Orha, C.; Pop, A.; Lazau, C.; Sfîrloagă, P.; Grozescu, I.; Tiponuţ, V.; Manea, F. Structural and Sorption Properties of Copper Doped Natural and Synthetic Zeolite. In Proceedings of the CAS 2011 Proceedings (2011 International Semiconductor Conference), Sinaia, Romania, 17–19 October 2011.

47. Tansel, B.; Sager, J.; Rector, T.; Garland, J.; Strayer, R.F.; Levine, L.; Roberts, M.; Hummerick, M.; Bauer, J. Significance of hydrated radius and hydration shells on ionic permeability during nanofiltration in dead end and cross flow modes. *Sep. Purif. Technol.* **2006**, *51*, 40–47. [CrossRef]

48. Munthali, M.W.; Johan, E.; Matsue, N. Proton Adsorption Selectivity of Zeolites in Aqueous Media: Effect of Exchangeable Cation Species of Zeolites. *Environments* **2015**, *2*, 91–104. [CrossRef]

49. Liu, Y. New insights into pseudo-second-order kinetic equation for adsorption. *Colloids Surf. A Physicochem. Eng. Asp.* **2008**, *320*, 275–278. [CrossRef]

50. Wang, J.; Guo, X. Adsorption kinetic models: Physical meanings, applications, and solving methods. *J. Hazard. Mater.* **2020**, *390*, 122156. [CrossRef]

51. Zendelska, A.; Golomeova, M.; Blazev, K.; Krstev, B.; Golomeov, B.; Krstev, A. Adsorption of copper ions from aqueous solutions on natural zeolite. *Environ. Prot. Eng.* **2015**, *41*, 17–36. [CrossRef]

52. Shen, X.; Qiu, G.; Yue, C.; Guo, M.; Zhang, M. Multiple copper adsorption and regeneration by zeolite 4A synthesized from bauxite tailings. *Environ. Sci. Pollut. Res.* **2017**, *24*, 21829–21835. [CrossRef]

53. Wang, S.; Wu, H. Environmental-benign utilisation of fly ash as low-cost adsorbents. *J. Hazard. Mater.* **2006**, *136*, 482–501. [CrossRef]

54. Tuyen, N.T.K.; Nhan, D.N.T.; Nhat, T.T.; An, N.T.; Long, N.Q. Removal of copper (II) ion from aqueous solution using zeolite Y synthesized from rice husk ash: Equilibrium and kinetic study. *AIP Publishing LLC* **2017**, *1878*, 20016. [CrossRef]

55. Kajjumba, G.W.; Emik, S.; Öngen, A.; Özcan, H.K.; Aydın, S. Modelling of Adsorption Kinetic Processes—Errors, Theory and Application. In *Advanced Sorption Process Applications*; Edebali, S., Ed.; IntechOpen: London, UK, 2018. [CrossRef]

56. Visa, M.; Popa, N. Adsorption of heavy metals cations onto zeolite material from aqueous solution. *J. Membr. Sci. Technol.* **2015**, *5*, 133–140.

57. Lu, X.; Shi, D.; Chen, J. Sorption of Cu^{2+} and Co^{2+} using zeolite synthesized from coal gangue: Isotherm and kinetic studies. *Environ. Earth Sci.* **2017**, *76*, 591. [CrossRef]

58. Motsi, T.; Rowson, N.A.; Simmons, M.J.H. Adsorption of heavy metals from acid mine drainage by natural zeolite. *Int. J. Miner. Process.* **2009**, *92*, 42–48. [CrossRef]

59. Komnitsas, K.; Zaharaki, D.; Pyliotis, I.; Vamvuka, D.; Bartzas, G. Assessment of Pistachio Shell Biochar Quality and Its Potential for Adsorption of Heavy Metals. *Waste Biomass Valorization* **2015**, *6*, 805–816. [CrossRef]

60. Ren, X.; Xiao, L.; Qu, R.; Liu, S.; Ye, D.; Song, H.-G.; Wu, W.; Zheng, C.; Wu, X.; Gao, X. Synthesis and characterization of a single phase zeolite A using coal fly ash. *RSC Adv.* **2018**, *8*, 42200–42209. [CrossRef]

61. Song, M.; Wei, Y.; Cai, S.; Yu, L.; Zhong, Z.; Jin, B. Study on adsorption properties and mechanism of Pb2+ with different carbon based adsorbents. *Sci. Total. Environ.* **2018**, *618*, 1416–1422. [CrossRef]

62. Townsend, R.P.; Coker, E.N. Chapter 11 Ion exchange in zeolites. *Sci. Technol. Catal. 2006* **2001**, *137*, 467–524. [CrossRef]

63. Chen, H.Y.; Chen, L.; Lin, J.; Tan, K.L.; Li, J. Copper Sites in Copper-Exchanged ZSM-5 for CO Activation and Methanol Synthesis: XPS and FTIR Studies. *Inorg. Chem.* **1997**, *36*, 1417–1423. [CrossRef]

64. Biesinger, M.C. Advanced analysis of copper X-ray photoelectron spectra. *Surf. Interface Anal.* **2017**, *49*, 1325–1334. [CrossRef]

65. Elzey, S.; Baltrusaitis, J.; Bian, S.-W.; Grassian, V.H. Formation of paratacamite nanomaterials via the conversion of aged and oxidized copper nanoparticles in hydrochloric acidic media. *J. Mater. Chem.* **2011**, *21*, 3162. [CrossRef]

66. Grünert, W.; Schlögl, R. Photoelectron Spectroscopy of Zeolites. In *Characterization I*; Karge, H.G., Weitkamp, J., Eds.; Springer: Berlin/Heidelberg, Germany, 2004; Volume 4, p. 492.

67. Zhang, M.; Yin, Q.; Ji, X.; Wang, F.; Gao, X.; Zhao, M. High and fast adsorption of Cd(II) and Pb(II) ions from aqueous solutions by a waste biomass based hydrogel. *Sci. Rep.* **2020**, *10*, 1–13. [CrossRef] [PubMed]

68. Payra, P.; Dutta, P.K. Zeolites: A Primer. In *Handbook of Zeolites Science and Technology*; Auerbach, S.M., Kathleen, A., Carrado, A., Dutta, P.K., Eds.; CRC Press: New York, NY, USA, 2003; pp. 1–19.

69. Pavelić, S.K.; Medica, J.S.; Gumbarević, D.; Filošević, A.; Pržulj, N.; Pavelić, K. Critical Review on Zeolite Clinoptilolite Safety and Medical Applications in vivo. *Front. Pharmacol.* **2018**, *9*, 9. [CrossRef]